PCCP

Accepted Manuscript

ROYAL SOCIETY OF CHEMISTRY

www.rsc.org/pccp

PCCP

RSCPublishing

ARTICLE

Cite this: DOI: 10.1039/xoxxoooooox

Understanding Adsorption of CO_2, N_2, CH_4 and its Mixture in Functionalized Carbon Nanopipe Array

Prosun Halder,[a), b)] Manish Maurya,[a), b)] Surendra K. Jain[a] and Jayant K. Singh[a]*,

Received ooth January 2012,
Accepted ooth January 2012

DOI: 10.1039/xoxxoooooox

www.rsc.org/

The selective adsorption behaviour of carbon dioxide, methane and nitrogen on bundles of functionalized CMK-5 are investigated at 303 K using grand-canonical Monte Carlo simulations. Functional groups (–OH, –COOH) cause a significant enhancement in CO_2 uptake (up to 19.5% at a pressure of 38.13 bar for –COOH). On the other hand, the adsorption amount of methane decreases with respect to bare CMK-5 by ~13% (at 38.13 bar) upon functionalization. Furthermore, functionalized CMK-5 with different pore sizes (4 nm, 6 nm, 8 nm) and inter-tube distances (d = 0 - 1.5 nm) are used to investigate the adsorption behaviour of flue gases. While pore diameter is seen to reduce the isosteric heat of adsorption, inter-tube distance of 0.25 nm shows the highest uptake of CO_2 at $p \leq 18$ bar, followed by 0.5 nm for the pressure range $18 < p \leq 30$ bar, whereas for $p > 30$ bar, d = 1.0 nm shows the maximum uptake. For methane and nitrogen maximum adsorption is obtained at d = 0.25 nm in the studied pressure range. Selective adsorption of CO_2 in binary mixtures is investigated using the ideal adsorption solution theory. CO_2-N_2 selectivity is found to increase significantly by surface functionalization of CMK-5 compare to pure CMK-5. The maximum selectivity of CO_2-CH_4 using –COOH functionalized CMK-5 is found to be ~10 for an equimolar CO_2-CH_4 mixture at a pressure 38.13 bar.

1. Introduction

Nanoporous carbon-based material has become the major attention in recent years because of their potential application as adsorbent, storage material[1, 2] etc. These nanoporous carbon-based materials are of great interest because of their high stability, high surface activity,[3] low cost and weight. However, it is very challenging to control the pore morphology and topology of the classically used activated carbons during their preparation process.[4] Hence, they do not possess a well ordered pores and uniform pore size. Some carbons such as fullerenes and single-wall nanotubes (SWNTs) exhibit periodic structures[5, 6] with voids potentially accessible to some adsorbate molecules. The periodically arranged fullerenes and SWNTs are held together via weak van der Waals interactions[5, 6] and thus can be considered as systems with permanent ordered porosity.[7] Recently, nanocasting using highly ordered mesoporous materials (like silica) has made possible to prepare novel mesostructured materials with permanent ordered porosity.[8] Ryoo et *al.* have shown that highly ordered mesoporous carbons can be obtained by templating highly ordered silica materials.[9] The template synthesis process to obtain mesoporous carbons is novel because it provides precise control of the porous structure of the final material. The structures of the carbons prepared in this way can be tailored by selecting the appropriate template material.[10] These carbon materials offer mechanical and thermal stability, high pore volume, electrical conductivity and useful surface properties. These materials are useful in various applications which include separation of unwanted molecules from aqueous or gaseous phase[11], catalysts in fuel cells and electrodes for capacitor.[12]

One of the important goals for the development of porous material is the separation/removal of CO_2, emitted in industrial and environmental processes, which is one of the main causes of global warming. While various works[13 14 15]have been done using liquid-gas absorption based method for the separation of CO_2, the method has inherent disadvantage such as low CO_2 loading, severe adsorbent corrosion and low contact area. On the other hand, capture of CO_2 on mesoporous surface is much more effective as summarized by Choi et *al.*[16] and Sayari et *al.*[17] in their excellent review on this topic. Plaza et *al.*[18] showed that activated carbon is a good adsorbent, which is widely available, and has high thermal stability. Though it has several favourable properties, its application is limited to high pressure gases. Zeolite is also reported as an adsorbent but it is not efficient because of its large size, charge density and chemical composition as shown by Wang et al.[19] Ordered mesoporous silica can be a good candidate because of its high surface area and highly ordered structure. Hence, several mesoporous silica materials (ex. M41S, SBA-15, AMS etc.) have been reported.[20-22] However, the adsorption isotherms are not comparatively high enough. In the last decade, metal-organic frameworks (MOFs) have been investigated intensively.[23-26], which showed exceptional adsorption capacities at high pressure for MOFs. However, at low pressure range the adsorption isotherms for CO_2 is less. Additionally, several reports indicate low selectivity towards CO_2 from the gas mixture.[27, 28]

Recently, covalent organic framework (COF) was introduced as a new class of porous material. Unlike MOFs, COF structures are entirely composed of light elements (H, B, C, and O). Furukawa et al. have synthesized and used several COFs for clean energy applications and found that COFs are among the most porous and the best adsorbent for CO_2, CH_4, and H_2.[29] Earlier studies show that the single-walled carbon nanotubes (SWCNT) can be used for adsorptive separation of CO_2.[30-33] Cinke et al.[30] found that the adsorption capacity is doubled for single-walled CNT compared to that of activated carbon. Hexagonally arranged multi walled carbon nanotubes (MWCNT) is also used to investigate the adsorption behaviour of carbon-dioxide.[34] Moreover, surface chemistry of these material can be tuned by adding functional groups or by altering the charge distribution of CNT to enhance the interaction.[35, 36]

Recently, a variety of porous material having a regular pore structure has been developed to expand the realm of materials suitable for clean energy applications and to curtail greenhouse effect. Among them, a porous material CMK-5 displays some unique properties including high surface area and large pore volume,[37, 38] making them favourable as an adsorbent. CMK stands for carbon material of Korea because the first template based porous material was synthesized by Ryoo et al.[9] Since then several CMK materials (up to CMK-9) has been synthesized till date using different templates and precursors during the synthesis.[39] Templated synthesis of ordered carbons can be done via volume-templated or surface-templated carbons. In the first case, the entire void space of the template is infiltrated with carbon, whereas in the second case, carbon is introduced as a film on the pore surface of the template. Volume templating method gives a rod like structure while surface templating gives a pipe like structure. Typical example of volume templating is CMK-3, in which carbon rods are arranged in a hexagonal symmetry. CMK-5 is the only surface templated carbon. There are two techniques widely used to enhance the adsorbate-adsorbent interaction: one is the fabrication of new porous material and other is via surface functionalization, which creates new surface active sites. In this study we have examined the effect of surface functionalization on CMK-5 on the adsorption behaviour of different flue gases, using molecular simulations.

2. Model and Methodology

2.1. MCM-41 Preparation

The MCM-41 pore is obtained by carving out a regular cylindrical pore of radius R_o in an atomistic block of cristobalite (a non-porous silica mineral) following the method first introduced by Pellenq et al. to prepare a numerical sample of nanoporous silica materials.[40] To mimic the pore surface in a realistic way, the Si atoms, which are in an incomplete tetrahedral environment, are removed. All these steps are done using an in-house code. In the second step, all oxygen atoms that are non-bonded are removed. This procedure ensured that the remaining silicon atoms have no dangling bonds and the remaining oxygen atoms have at least one saturated bond with a Si atom. Subsequently, the electro-neutrality of the simulation box is ensured by saturating all oxygen-dangling bonds with hydrogen atoms. The hydrogen atoms are placed in the pore void, perpendicularly to the pore surface at a distance of 1 Å from the closest unsaturated oxygen atom. The structure is further relaxed by performing Monte Carlo simulations in the NVT ensemble using an in-house code at a high temperature. More details regarding the MCM-41 pore model can be found in the work of Coasne et al.[41] The MCM-41 pore model used in our work has a pore diameter of 28 Å, 8398 atoms, and a pore length of 106.95 Å. A snapshot of the top and front view of the pore is shown in Figure 1.

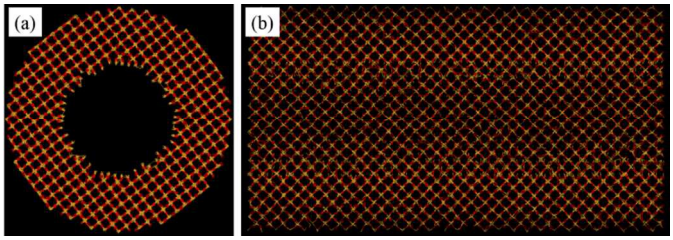

Fig. 1. The top view (a) and front view (b) of the MCM-41 pore.

The above MCM-41 structure is used as a template for carbon adsorption. The interaction between adsorbate (the carbon atoms) with the silica matrix is assumed to be weak and in the physisorption energy range. The interaction energy is calculated using the PN-TrAZ potential, a simplified version of the original PN-type potential function as reported for adsorption of rare gases and nitrogen in silicalite-1.[42]
The interaction between the carbon atoms is calculated using the Reactive Empirical Bond Order (REBO) potential of Brenner.[43] The energy between two carbon atoms i and j is calculated using

$$U_{ij} = V_{ij}^{R}\left(r_{ij}\right) + b_{ij}V_{ij}^{A}\left(r_{ij}\right), \quad (1)$$

where V_{ij} is a pair repulsive and V_{ij}^{A} is a pair attractive term and b_{ij} is a bond order term, which weights the attractive part of the potential with respect to the repulsive part. The bond order term is a many body term, which depends on the local environment of atoms i and j.

2.2. Adsorption on CMK-5 surface

The intermolecular interaction energy between two molecules is expressed below:

$$E = 4\varepsilon_{ij}\left[\left(\frac{\sigma_{ij}}{r_{ij}}\right)^{12} - \left(\frac{\sigma_{ij}}{r_{ij}}\right)^{6}\right] + \frac{Cq_iq_j}{\varepsilon r_{ij}}. \quad (2)$$

The first term in the right hand side of equation 2 represents the standard 12-6 Lennard-Jones potential and the second term is the Columbic pairwise interactions between site i and site j of two different molecules.

The potential parameters for CMK-5 are taken from Peng et al. (2009).[44] N_2 is modeled by TraPPE force field proposed by Potoff et al.[45], whereas CH_4 molecule is modeled as four-site model.[46] CH_4 potential parameters are taken from OPLS model of Jorgensen et al. (1990).[47] In case of CO_2, EPM2 model of Harris and Yung[48] is used. All the molecules are considered as rigid; hence the bond bending potential is not included. Interaction parameters for different atoms are listed in Table 1. The Lennard-Jones interactions between unlike atoms are approximated using Lorentz-Berthelot rules.[49] Interaction between two molecules beyond 1 nm is neglected to reduce the computational time. The number of atoms is varied from 16000 to 80000.

Table 1. Interaction parameters of adsorbates and CMK-5 adsorbent[44, 47, 48]

Species	Site	σ (nm)	ε (kcal/mol)	q (e)
CO_2	C	0.2757	0.0559	0.6512
	O	0.3033	0.16	-0.3256
N in (N_2)	N	3.31	0.072	-0.482
COM (in N_2)	N	0.0	0.0	0.964
CH_4	C	0.35	0.066	-0.24
	H	0.25	0.03	0.06
CMK-5	C	0.336	0.0556	0.0

2.3. Adsorption Theory

The adsorption or surface excess of a given component is defined as the difference between the amount of component actually present in the system, and that which would be present (in a reference system) if the bulk concentration in the adjoining phases were maintained up to a chosen geometrical dividing surface. Thus absolute adsorption amount is converted into excess adsorption of adsorbate using equation 3.

$$N_{ex} = N_{ad} - \rho_b V_{free}, \quad (3)$$

where N_{ex}, N_{ad} are the excess and absolute adsorption amounts, respectively. ρ_b is the bulk density of the adsorbate and V_{free} is the accessible volume for gas particles. Bulk density can be calculated by performing independent grand-canonical Monte Carlo (GCMC) simulations at different chemical potential. There are various methods to calculate the free volume.[50-52] In this work, free volume is calculated using Helium (He) adsorption technique.[53]

The adsorptive characteristics of an adsorbent can also be analysed by studying the strength of the adsorbent-adsorbate interaction that is given by the heat of adsorption, which can be obtained from GCMC simulations. Isosteric heat of adsorption[54] (q_{st}) is usually expressed in the approximated form as:

$$q_{st} \approx RT - \left(\frac{\partial U_{ad}}{\partial N_{ad}} \right)_{T,V}, \quad (4)$$

where U_{ad} is the potential energy of the adsorbed phase. Equation 4 further can be modified in the form given below:

$$q_{st} = RT - \frac{\langle U_{ad} N_{ad} \rangle - \langle U_{ad} \rangle \langle N_{ad} \rangle}{\langle N_{ad}^2 \rangle - \langle N_{ad} \rangle^2}, \quad (5)$$

where, angled bracket represents an ensemble average.
Adsorption selectivity in a binary mixture of component *i* and *j* is defined as

$$S_{i/j} = \left(\frac{x_i}{x_j} \right) \left(\frac{y_j}{y_i} \right). \quad (6)$$

Where x_i and y_i are the mole fractions of component i in the adsorbed and bulk phases, respectively.

3. Simulation details

3.1. CMK-5 Preparation

We start with a MCM-41 cylindrical pore model as a template for our CMK-5 model. We subsequently performed GCMC simulation for the adsorption of carbon atoms in MCM-41 pore model of diameter 28 Å and a length of 106.95 Å, as shown in figure 2a. In the usual experimental procedure for CMK-5 preparation, first adsorption of a polymer inside the silica template is performed. This is followed by carbonization (heating at high temperature) and removal of silica template. We avoid following the exact experimental procedure, as the interest is in the final structure of the porous matrix. Thus, in this molecular simulation work, the carbon atoms are first adsorbed in the MCM-41 pore. This is achieved at a high temperature of 3000 K, as at lower temperature the adsorption process of carbon atoms is not efficient due to low acceptance ratio. The GCMC code for the development of the CMK-5 (using REBO potential for interaction between carbon atoms and PNTraz potential for interaction between silica and carbon atoms) was developed in the group of Keith Gubbins at NCSU. Periodic boundary conditions are assumed only along the pore axis (X-axis) to get the cylindrical pipe shape. In order to speed up the simulation, we divided the simulation box into a fine grid of 100 × 100 × 100 and calculated the interaction of one adsorbate (carbon) atom with the adsorbent (MCM-41 silica) at each grid point. During the GCMC simulation the adsorbate-adsorbent potential energy is calculated using a trilinear interpolation in the energy grid. Starting with many carbon dimers located near the pore surface, we gradually raised the chemical potential and recorded the average number of adsorbed carbon atoms. We stop the simulation when we reached to the specified pore width of carbon atoms inside the MCM-41 pore, which decides the diameter of the CMK-5. We then remove the MCM-41 silica template and obtain the final carbon structures (pipes) that are roughly cylindrical. These carbon structures (individual carbon pipes) are then relaxed (relaxed in NVT ensemble) with the REBO potential. Radial distribution function of the C-C atoms of this material can be found in the supporting information (S1). Since experimentally[37] obtained CMK-5 is hexagonally arranged, we place the final relaxed individual amorphous carbon pipe on a hexagonal lattice using VMD (Visual molecular dynamics) software[55] to obtain CMK-5 models with different inter tube distances. The inter-tube distance results are obtained assuming periodic structure of CMK-5, though the basic structure is highly amorphous. CMK-5 is the carbon material having carbon nanopipes arranged in hexagonal symmetry. So, in this work CMK-5 refers to all the models in which carbon pipes are arranged in hexagonal symmetry (irrespective of tube diameters and inter tube distances)..

The final CMK-5 structures are amorphous as the carbon atoms are present in a disordered configuration. We emphasize that we are not

mimicking the synthesis process in our simulations. In reality, a carbon precursor is infiltrated into the silica template and is then polymerized and carbonized to obtain the carbon. In our case, we are not simulating the polymerization or carbonization process as we are interested in the final carbon structure only. By simulating the carbon adsorption in a silica pore, we obtain a carbon structure that resembles and contains the features of a realistic carbon replica obtained from a silica template.

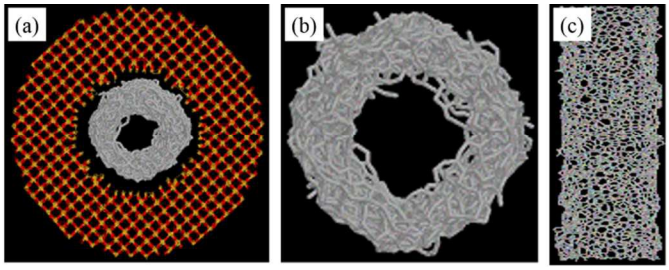

Fig. 2. (a) Carbon pipe obtained by doing carbon adsorption in the MCM-41 pore. Carbon pipe obtained after removing the silica template and relaxing the carbon structure: (b) top view and (c) side view.

The carbon-silica (fluid-wall) potential energy in our case is physisorption energy, and thus is much smaller in magnitude as compared to carbon-carbon (fluid-fluid) energy that involves formation of a covalent bond. Thus, the wetting of the silica surface by carbon atoms is not observed which is necessary to obtain carbon pipes. Hence, we increase the fluid-wall potential energy at each grid point by multiplying the fluid-wall energy obtained with the PN-Traz potential[42] with a fixed integer. The use of the reactive REBO potential ensures that the chemistry of the carbon atoms is correctly reproduced at the local level. The final carbon structures (carbon nanopipes) consists of rings (5,6,7 membered) of carbon atoms as found in microporous carbon models[56, 57]. Final structure of CMK-5 is shown in figure 2b and 2c.

3.2. Functionalization

We added different functional groups to our arrays of carbon nanopipes to study the effect of functional groups on adsorption. The method to add functional groups is as follows: we randomly select a carbon atom and add a functional group in the radial direction perpendicular to pore wall. We then check for overlap of the functional group with other carbon atoms of the matrix and with other functional groups already added. If there is an overlap, we do not add the functional group and randomly select another carbon atom to add the functional group.

Table 2. Interaction parameters of functional groups[58]

Group	Site	σ (nm)	ε (kcal/mol)	q (e)
Hydroxyl	C[a]			0.2
	O	0.307	0.1554	-0.64
	H			0.44
Carboxyl	C[a]			0.08
	C	0.375	0.1033	0.55
	O	0.296	0.21	-0.5
	O	0.3	0.1701	-0.58
	H			0.45

C[a] is the Carbon located in plane of nanopipe surface.

Functional groups are attached to the internal surface as well as to the external surface of carbon nanopipes. In this work, two different groups are used, namely carboxyl (-COOH) and hydroxyl (-OH) groups. The distance, angle and potential parameters are tabulated in Table 2. We have varied the percentage of functionalization (by weight) from 2% to 5%.

3.3. Simulation set-up

Figure 3 shows the schematic of micro-porous nanopipes in a unit cell where nanopipes are arranged on a hexagonal lattice. The simulation box is periodic in all three directions. Since the diameter of the tube is not constant, the external diameter is used for obtaining the cell dimension. Different inter-tube distances *viz*., 0 nm, 0.25 nm, 0.5 nm, 1 nm, and 1.5 nm have been used to analyse the effect of porosity. In a unit cell two nanopipes are placed to observe adsorption on internal nanopipe surface as well as external nanopipe surface. The length of unit cell in the direction of nanopipe axis is fixed at 8.14 nm. The rest of the dimensions of unit cell are adjusted using the external diameter of nanopipe and inter-tube distance. GCMC simulations are conducted to study the adsorption of various gas molecules. Carbon-dioxide, methane and nitrogen are used as adsorbate for this adsorption simulation. The temperature and volume of the simulation box are kept constant. Multiple simulations are conducted using different chemical potential values to generate the adsorption isotherm. Pressure calculation can be found in the supporting information (S2). Since flue gas is generally cool down to 25 ^{o}C - 30 ^{o}C before the removal of CO_2, we have fixed the temperature to 303 K for the current study. Three Monte Carlo (MC) moves are employed in the simulation. The probabilities for different moves are 0.2 for translation move, 0.1 for rotational move, 0.7 for addition/deletion move. Each GCMC simulation consists of equilibration run of 2.5 x 10^7 MC steps and an equal amount for the production run.

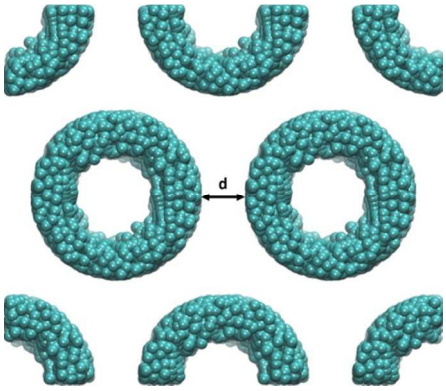

Fig. 3. Schematic arrangement of CMK-5 used in GCMC simulation, with an inter-tube distance *d*.

4. Results and discussion

4.1. Adsorption on pure CMK-5

We start the discussion with the adsorption isotherms of pure CO_2, CH_4 and N_2 on the bare CMK surface as shown in Figure 4.

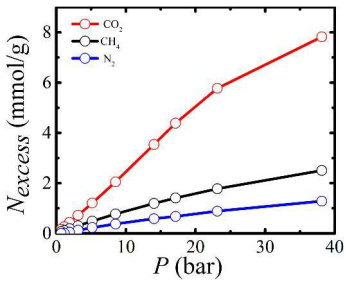

Fig. 4. Excess adsorption isotherms of CO_2, CH_4, N_2 in bare CMK-5 arrays with tube diameter 4 nm, inter-tube distance 1 nm at T = 303 K.

The excess adsorption increases with pressure, as expected, for all the three gases considered in this work, though the behavior is dependent on the type of gas molecules. While CO_2 is more favorable as an adsorbate, which reaches up to 7.8 mmol/g at P = 38.14 bar, the corresponding values for N_2 and CH_4 are ~1.5 and 2.5 mmol/g respectively. The amount of gas uptake is in the order of $N_2 < CH_4 < CO_2$, which is in accordance to its interaction strength with CMK-5. To have a better understanding of the adsorption behavior, local density is presented in figure 5. Two distinguishable peaks are observed next to the inside and outside of the pore wall, for each case, indicating monolayer adsorption of gas molecule on the nanopipe wall. The pronounced adsorption with increase in pressure is evident in the increase in the peak height of the density profile with pressure. Furthermore, it is clear that adsorption, for $P \le 23.13$ bar, occurs within the first layer next to the CMK-5 surface. Nevertheless, second layer initiate to form at higher pressure. At lower pressures the peak height inside the pore is higher than the peak height in the inter-tube region. However, at higher pressure the peak heights are almost similar.

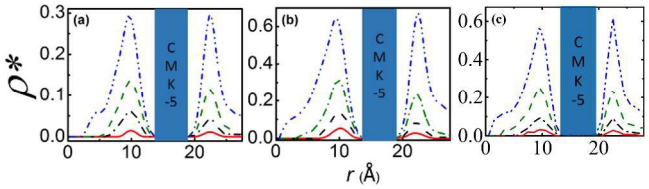

Fig. 5. Local density profile of (a) CH_4, (b) CO_2, (C) N_2 adsorbed on the surface of pore wall. Here, r is the distance from the nanopipe center. The dash dot doted, dashed, dash doted, straight lines represent the density profiles at 23.13, 8.51, 3.13, 1.15 bar, respectively.

4.2. Adsorption on functionalized CMK-5

Figure 6a presents the effect of carboxyl and hydroxyl functionalized CMK-5 on the adsorption isotherms of CO_2, CH_4 and N_2. For all gases, carboxylic group functionalized CMK-5 shows much more affinity for adsorption than hydroxyl group functionalized CMK-5.

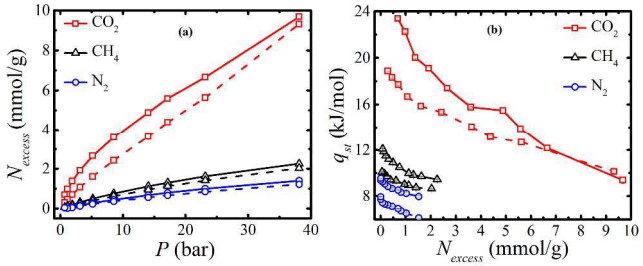

Fig. 6. (a) Excess adsorption of CO_2, CH_4, N_2 as a function of pressure and (b) heat of adsorption as a function of excess adsorption in functionalized CMK-5 arrays with pore diameter 4 nm and inter-tube distance 1.0 nm, at 303 K. Solid and dashed lines represent adsorption in carboxyl group and hydroxyl group (4 % by weight) functionalized CMK-5, respectively.

At higher pressures, for CO_2, the excess adsorption is comparatively higher for both carboxyl group functionalized CMK-5 and hydroxyl group functionalized CMK-5 than for pure CMK-5. At P = 38.14 bar excess adsorption isotherm of carbon dioxide is 9.7 mmol/g (for pure CMK-5 it is ~8 mmol/g). However, in case of methane, the excess adsorption isotherm, at higher values of pressure, is less than that seen for the bare CMK-5. The binding energy or effective interaction strength of gas molecules with CMK-5 can be interpreted from q_{st} when number of gas molecule approaches zero (see equation 4). Hence, higher q_{st} at lower value of N_{excess} indicate higher interaction strength of the gas molecule with the CMK-5. The corresponding values for nitrogen and CO_2 are ~10 kJ/mol and ~24 kJ/mol, respectively. This supports the observation of low amount of adsorption for nitrogen. The effect of the functional group is also reflected in the heat of adsorption as shown in figure 6b. In most cases, the q_{st} monotonically decrease with increase in the adsorption amount, which is expected (until the saturation of monolayer). In case of carboxyl group functionalized CMK-5, the interaction strength is higher than that for hydroxyl group functionalized nanopipes for all adsorbates. For further investigation, snapshots of carbon-dioxide, methane and nitrogen in different functionalized CMK-5 are presented in figure 7.

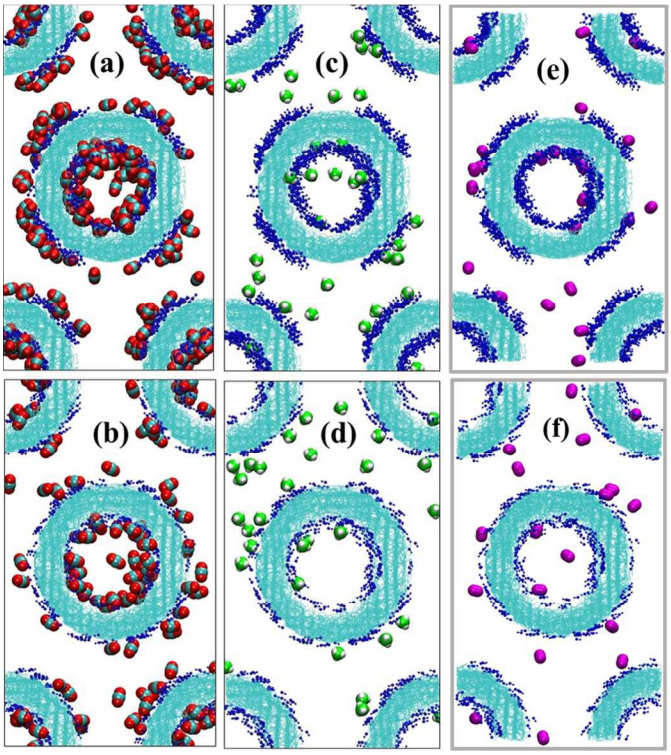

Fig. 7. Snapshots of CO_2 (a,b), CH_4 (c,d), N_2 (e,f) in 4% -COOH (Top) and -OH (bottom) functionalized CMK-5 arrays, having 4 nm diameter and 1 nm inter-tube distance, at 1.15 bar and 303 K. Blue color represent functional groups attached to CMK-5.

The snapshots illustrate that at a given pressure the adsorption amount for all the gases is higher for –COOH functionalized nanopipes than –OH functionalized nanopipes. It is observed that –COOH functionalization allows filling the monolayer within the interior section of the pore as opposed to the –OH functionalized CMK-5. The snapshot also reveals that CO_2 has the strongest interaction with functionalized CMK-5 as depicted by the enriched amount of adsorption within the pore. While the –OH group also cause significant adsorption as observed by the appearance of second layer for the case of CO_2, the effect is not as pronounced as seen for –COOH. After functionalization density of CO_2 slightly increases inside the CMK-5 compare to outside of CMK-5. The behavior is attributed mainly to the increased density for the functional group within the pore leading to preferential adsorption inside the pore. Hence, the density inside the pore increases with increasing pressure. This is also evident from the snapshots as shown in Fig 7.

4.3. Effect of different concentration of functionalization

Now, we turn our attention to the effect of different amount of functionalization on excess adsorption and heat of adsorption. Figure 8 (top) presents the excess adsorption of CO_2, CH_4, N_2 for different percentage of carboxylic group functionalized CMK-5. In case of carbon dioxide the excess adsorption increases with increaing amount of –COOH group. However, relatively negligible amount of enhancement of excess adsorption is seen for methane and nitrogen (particularly at low pressure). Since interaction strength of methane and nitrogen with both functional groups is weak, the increase in percentage functionalization does not cause significant enhancment in their adsorption amount. However, the heat of adsorption, for –COOH functional CMK-5, show some significant change, as seen in figure 8 (bottom). At a lower pressure the electrostatic and dispersion interactions between carbon dioxide molecules and –COOH group play a major role leading to significant enhancement of the heat of adsoption (at lower value of excess adsorption), which is seen releatively less for CH_4 and N_2.This can be seen in the snapshot given in the supporting information (S3).

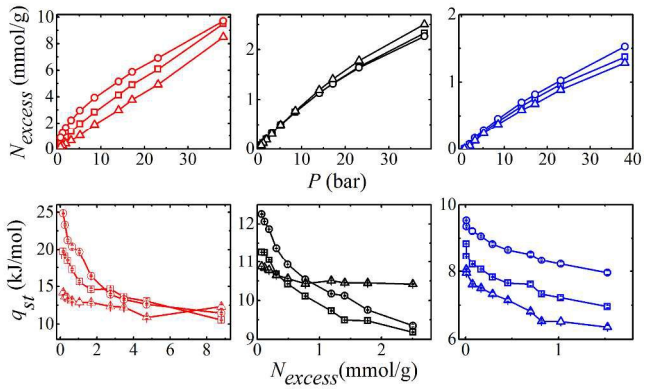

Fig. 8. Excess adsorption isotherm (top) and Isosteric heat of adsorption (bottom) of CO_2 (red), CH_4 (black), N_2 (blue) in –COOH group functionalized CMK-5 with 4 nm pore size and 1 nm inter-tube distance respectively. Symbols, up triangle, square, and circle are representing pure CMK-5, 2% -COOH functionalize CMK-5, and 5% -COOH functionalized CMK-5, respectively.

Figure 9 presents the excess adsorption and heat of adsorption for CO_2, CH_4, N_2, in hydroxyl functionalized CMK-5. For methane and nitrogen, slight deviation in adsorption isotherm from pure CMK-5 is seen with increase in the amount of functional group, which is also supported by the isosteric heat of adsorption. This is attributed to the less attraction of methane and nitrogen towards the functional group. With increasing percentage functionalization, the active sites decrease for methane and nitrogen molecules leading to decrease in the adsorption amount. In case of nitrogen the effect is extremely small, and can be neglected for the given pressure range. Meanwhile, for CO_2, the excess adsorption increases slightly with the introduction of additional –OH functional group due to the stronger interaction strength of CO_2 with the functional group unlike that for methane and nitrogen.

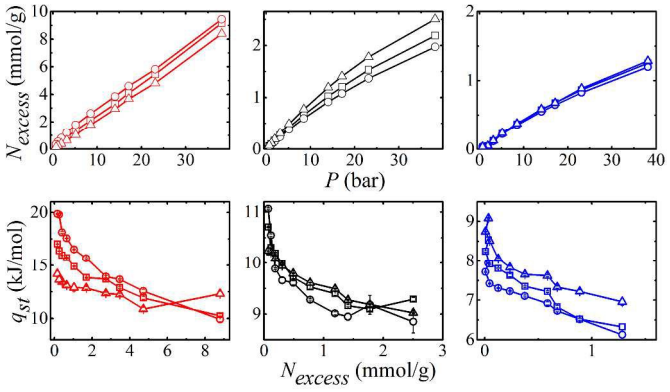

Fig. 9. Excess adsorption isotherm (top) and Isosteric heat of adsorption (bottom) of CO_2 (red), CH_4 (black), N_2 (blue) in –OH group functionalized CMK-5, with 4 nm pore diameter and 1 nm

inter-tube distance, respectively. Symbols, up triangle, square, and circle represent pure CMK-5, 2% functionalized CMK-5, and 5% functionalized CMK-5, respectively.

In comparison with the adsorption amount for the gas molecules in pure CMK-5, the adsorption amount for CO_2 is found to increase significantly with the introduction of more carboxyl groups. For example, 5 wt % functionalized CMK-5 with -COOH group enhances the amount of adsorption of CO_2 by 19.5% On the other hand, for methane the situation is quite opposite for –OH functionalized CMK-5 i.e. the presence of more functional groups leads to the decrease in the adsorption amount such that for 5 wt % -OH functionalized CMK-5 ~13% reduction in the excess adsorption is seen compared to bare CMK-5. The CO_2 capacity of functionalized CMK-5 with -COOH and –OH groups reaches to 9.7 and 9.4 mmol/g at ~38 bar and 303 K respectively, which is close to the experimental CO_2 uptake of CMK-3 (10.5 mmol/g at 298 K) using similar hexagonal arrangements[59]. However, our results differ from that of Peng et *al*.[60] who obtained CO_2 capacity of 28 mmol/g at 40 bar, 298 K on bare CMK-5, which is significantly higher than the corresponding value in our case (8.5 mmol/g at 38 bar and 303 K in bare CMK-5). It is noted that the models used in this work and by Peng et *al.* are dramatically different. While, we have considered all atom approach, Peng et *al*. considered non-structured surface for CMK-5 and single site bead for fluid molecules. We believe that the difference in the models may be reason for the discrepancy.

4.4. Effect of pore diameter

Since adsorption behavior depends on structure and geometrical size of a material, we have studied the effect of pore size of CMK-5 on the separation and storage of flue gases. Here we used three different pore sizes *viz*., 4 nm, 6 nm and 8 nm. We show that for any operating storage pressure, there is a unique size of nanopipe that maximizes the overall gravimetric uptake of a flue gas. The excess adsorption isotherms for 2% carboxylic group functionalized CMK-5 having different diameters and a constant inter-tube distance of 1.0 nm are given in figure 10.

It is evident from figure 10 that as the pore diameter is increased the excess adsorption decreases though absolute adsorption would still increase[61, 62] as it can be seen in figure 11. The uptake of each pure gas decreases with increasing diameter due to increase in curvature of CMK-5. This in turn resulted in decrease in local density of adsorbate molecule around the adsorbent molecule becauses of less interaction with the adsorbate. As the pore diameter increases from 4 nm to 6 nm a significant drop in the excess adsorption is seen. However, the decrease in excess adsorption is not much when the diameter increases from 6 nm to 8 nm. Similar behavior has been seen by earlier workers[63]. The effect of diameter is also noticed on the isosteric heat of adsorption as shown in figure 10 (bottom). We observe that isosteric heat of adsorption decreases with increasing pore width. This phenomenon can be explained in terms of the interactions between the fluid-fluid and the fluid solid molecules. Fluid –fluid interaction dominates at high loading because of greater number of neighboring adsorbed molecules. While solid-fluid interactions dominate at low loading because of the overlapping of solid-fluid potential from both neighboring and opposite solid pore molecules. At higher pore width contribution from opposite pore wall reduces, and hence total isosteric heat of adsorption decreases with pore width. Similar observations are by Peng et al.[64] q_{st} typically decreases with excess adsorption until the saturation of the monolayer (or before the initiation of second or higher layers). The effect of diameter is not seen much at lower pressure or lower values of adsorption on q_{st}.

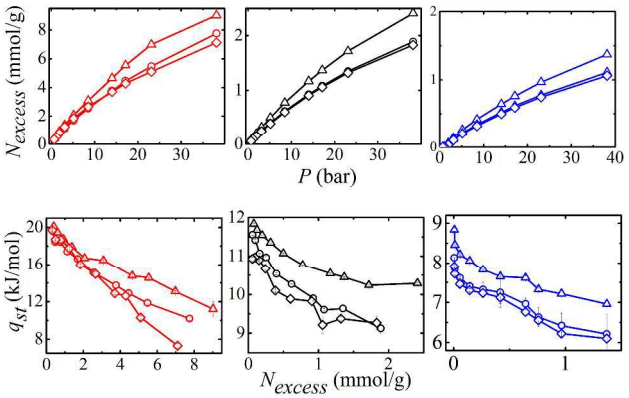

Fig. 10. Excess adsorption isotherm of (a) Carbon dioxide, (b) Methane, (c) Nitrogen in 2% carboxylic group functionalized CMK-5, with 1 nm inter-tube distance, at 303 K, respectively. Symbols, triangle, circle, and diamond represent 4 nm, 6nm, and 8nm diameter, respectively.

4.5. Effect of Intertube distance on adsorption

Figure 12 shows the adsorption isotherms of CO_2, CH_4 and N_2 for different intertube distances (d = 0 - 1.5 nm) on bare CMK-5. At lower intertube distance, the isotherm saturates at lower values of pressure. This is mainly due to less volume available for adsorption. However, with increase in the intertube distance the saturation occurs at higher pressures. This is evident for the case of CO_2 within the pressure range studied in this work. The intertube distance affects the excess adsorption by affecting the groove regions. At lower intertube distance the grooves are the preferred adsorption regions, which is not the case for higher intertube distance leading to a crossover behavior of adsorption isotherm. Intertube distance of 0.25 nm shows the highest uptake of CO_2 up to pressure $\leq$ 18 bar followed by 0.5 nm intertube distance for the pressure range of 18 < $p \leq$ 30 bar. For all other pressure $p \geq$ 30 bar, the maximum uptake of CO_2 is observed at d = 1.0 nm. For methane and nitrogen, the maximum adsorption is observed at d = 0.25 nm in the studied pressure range.

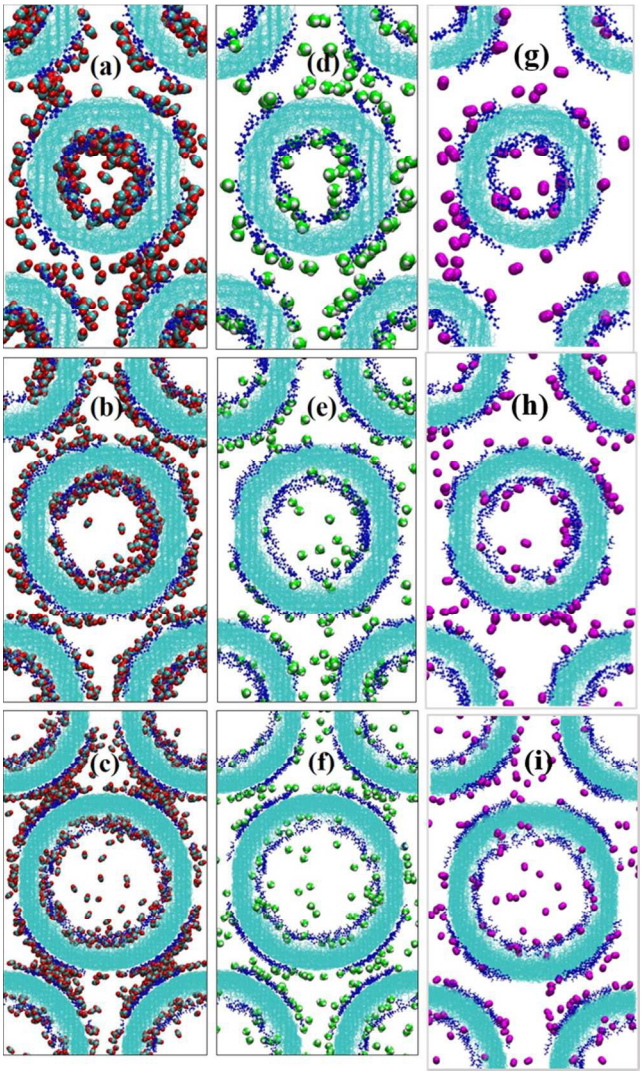

Fig. 11. Snapshots of absolute loading of CO_2 (a, b, c), CH_4 (d, e, f), and N_2 (g, h, i) in 2% functionalized CMK-5 of diameter 4, 6, 8 nm respectively at 3.13 bar, 303 K. Blue color represent attached functional groups to CMK-5.

For methane and nitrogen gases the maximum uptake is observed at d = 0.25 nm due to enhanced adsorption in the groove regions. However, with further increase in the intertube distance, the amount of adsorption decreases due to weak affinity of methane and nitrogen gases with CMK-5 carbon atoms. Nevertheless, the effect of intertube distance is relatively less for CH_4 and N_2 compared to that seen for CO_2.

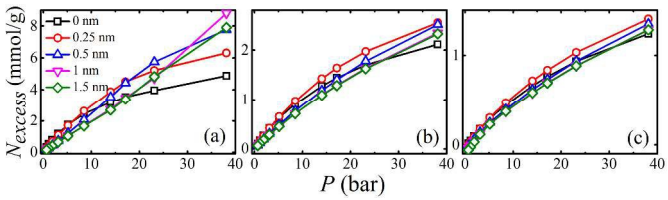

Fig. 12. Effect of different intertube distance of bare CMK-5 on adsorption capacity of (a) CO_2, (b) CH_4, and (c) N_2

4.6. Fitting of adsorption isotherms from GCMC simulations

In order to predict the adsorption isotherms of binary mixtures, we first fit the adsorption isotherms of pure components using Langmuir isotherm equation The model parameters obtained from the fit, for different adsorbates, in functionalized CMK-5s are tabulated in table 3. In order to predict the adsorption behavior of binary gas mixture, we used IAST that utilizes the absolute adsorption isotherms of pure components. In this work, we estimate the adsorption isotherms of 3 types of equimolar binary mixtures, *viz*. CO_2-CH_4, CH_4-N_2, CO_2-N_2. Figure 13 presents the total adsorption amount of different binary gas mixtures in the functionalized CMK-5. The trends observed for the adsorption isotherms of different gases in the mixtures are similar to that observed for the pure component isotherms. The CO_2 adsorption capacity is the highest for COOH functionalization. Adsorption uptake can be analyzed by the Langmuir's constants listed in Table 3. The values of Langmuir's constant correlate well with the maximum monolayer capacities of the OH and COOH functionalized CMK-5.

Table 3: Model parameters for Langmuir isotherm equation obtained by fitting absolute adsorption isotherms from GCMC simulations. q is monolayer capacity (mmol/g) and k is Langmuir constant (bar^{-1}).

Component	Pore diameter (nm)	% functionalization	Inter-tube distance (nm)	CMK-5 Functionalization			
				-OH		-COOH	
				q	***k***	***q***	***k***
CO_2	4	2	0.5	25.071	0.015	9.66	0.063
	6	4	1.0	9.192	0.042	7.22	0.135
	8	5	1.5	9.139	0.047	6.26	0.233
CH_4	4	2	0.5	8.494	0.014	6.76	0.02
	6	4	1.0	8.748	0.011	5.94	0.021
	8	5	1.5	10.122	0.01	6.13	0.022
N_2	4	2	0.5	0.97	0.03	1.98	0.019
	6	4	1.0	0.253	0.05	1.15	0.026
	8	5	1.5	0.085	0.07	1.01	0.03

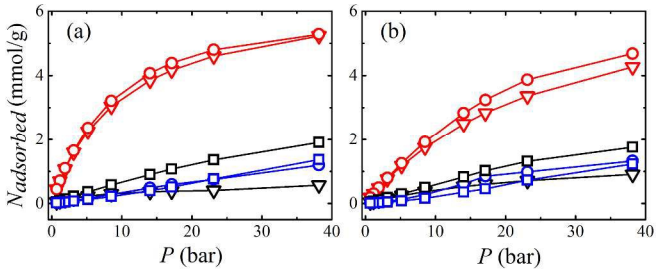

Fig. 13. Adsorption isotherm of equimolar mixture by IAST prediction in 5% (a) –COOH, (b) –OH functionalized CMK-5 with diameter of 4 nm and inter-tube distance 1.5 nm. Symbols down triangle, circle, and square represent CO_2/CH_4, CO_2/N_2 and CH_4/N_2 mixture respectively. Colors red, black and blue represent CO_2, CH_4 and N_2, respectively.

Furthermore, we also observed that the adsorption rate is high for COOH functionalization compare to OH functionalization as the surface saturates more quickly for the COOH modified surface. The IAST data is used to examine the selectivity of different functionalized CMK-5, which is shown in figure 14.

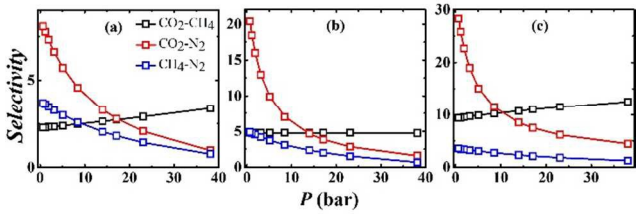

Fig. 14. Selectivity of equimolar mixture by IAST prediction in bare CMK-5 (a) and 5% (b) –OH, (c) –COOH functionalized CMK-5 with diameter of 4 nm and inter-tube distance of 1 nm.

It is observed that the selectivity of –COOH functionalized CMK-5 is more towards carbon dioxide than the other gases. The selectivity for the mixtures studied in this work follows the order $S_{CH_4-N_2} < S_{CO_2-CH_4} < S_{CO_2-N_2}$. For the CH_4-N_2 binary mixtures, the selectivity varies in the range 2-5 and it increases slightly upon functionalization.

In case of CO_2-CH_4 mixture in –COOH functionalized CMK-5, the selectivity towards CO_2-CH_4 is ~10 at P ~38 bar, which is around 2 times higher than the bare CMK-5. Selectivity increases significantly for CO_2-N_2 mixture after functionalization of CMK-5 with –OH and –COOH groups. The current study suggests that while CO_2 adsorption capacity of CMK-5 is not enhanced dramatically, the selectively however is significantly higher (200%) for –COOH functionalized CMK-5. This is primary due to the effect of –COOH, which leads to enhancement of CO_2 adsorption on one hand and diminution in the adsorption capacity of other gases leading to higher selectively for CO_2. Hence, CMK-5 with COOH functionalization is a suitable material for efficient gas separation.

5. Conclusions

Adsorption mechanisms of CO_2, CH_4, N_2 on functionalized CMK-5 arrays were investigated using GCMC simulations. Langmuir isotherm model was found to fit extremely well the adsorption isotherms. The adsorption behavior was analyzed using adsorption isotherm, local density distribution and isosteric heat of adsorption of pure gases. It was observed that functionalization could affect the adsorption isotherms. More precisely, due to the functionalization the uptake increases for CO_2 however it slightly decreases for CH_4. On the other hand, for nitrogen negligible enhancement can be seen for –COOH functionalization. In terms of adsorption capacity, –COOH functionalized CMK-5 was much more favorable than –OH functionalized CMK-5. Moreover, it was observed that the pore diameter plays a major role in adsorption isotherms for pure gases. For all adsorbates, excess adsorption isotherm decreases with increasing pore diameter. The effect of inter-tube distance was found to be negligible on the adsorption behavior of flue gases. Intertube spacing also affects the excess adsorption of CO_2, CH_4, and N_2. For low pressure, p ≤ 18 bar, maximum adsorption was observed for d = 0.25 nm followed by d = 0.5 nm in the pressure range, 18 < p ≤ 30 bar. However, for p > 30 bar maximum adsorption was observed at d = 1.0 nm. For methane and nitrogen maximum uptake was found at d = 0.25 nm in studied pressure range.

The adsorption mechanism was further investigated for the equimolar binary mixtures of CO_2-CH_4, CO_2-N_2 and CH_4-N_2. The selectivity of these gases was predicted using the IAST theory. For CO_2-CH_4 binary mixture the selectivity of CO_2 was highest for –COOH functionalized CMK-5 system. The selectivity was found to follow the order: $S_{CH_4-N_2} < S_{CO_2-CH_4} < S_{CO_2-N_2}$ Considering the two times higher selectivity of CO_2 with other gases for–COOH functionalized CMK-5 as opposed to the bare CMK-5, CMK-5 with COOH functionalization was found to be a suitable adsorbent for an efficient gas separation.

Acknowledgement

This work has been supported by Ministry of Earth Sciences, Govt. of India. The computational facility was provided by HPC, Computer Centre, Indian Institute of Technology Kanpur.

Notes and references

[a] Department of Chemical Engineering, Indian Institute of Technology Kanpur, Kanpur-208016, India

[b] Prosun Halder and Manish Maurya contributed equally to this work.

* Corresponding author. E-mail: jayantks@iitk.ac.in Phone: +91-512-2596141, Fax: 91-512-2590104

† Electronic Supplementary Information (ESI) available: [details of any supplementary information available should be included here]. See DOI: 10.1039/b000000x/

1. H. Kabbour, T. F. Baumann, J. J. H. Satcher, A. Saulnier and C. C. Ahn, *Chem. Mater.*, 2006, 18, 6085.
2. Z. X. Yang, Y. D. Xia and R. J. Mokaya, *Am. Chem. Soc.*, 2007, 129, 1673.
3. S. J. Gregg and K. S. W. Sing, *Adsorption, Surface Area and Porosity*, Academic Press: London, 2nd edn., 1982.

4. T. Kyotani, *Carbon*, 2000, 38, 269.
5. P. A. Heiley, *J. Phys. Chem. Solids.*, 1992, 53, 1333.
6. A. Thess, R. Lee, P. Nikolaev, H. Dai, P. Petit, J. Robert, C. Xu, Y. H. Lee, S. G. Kim, D. T. Colbert, G. E. Scuseria, D. Tomanek, J. E. Fisher and R. E. Smalley, *Science*, 1996, 273, 483
7. Q. Song, S. Jiang, T. Hasell, M. Liu, S. Sun, A. K. Cheetham, E. Sivaniah and A. I. Cooper, *Adv Mater*, 2016, DOI: 10.1002/adma.201505688.
8. H. Yang and D. Zhao, *J. Mater. Chem.*, 2005, 15, 1217.
9. R. Ryoo, S. H. Joo and S. J. Jun, *Phys.Chem. B*, 1999, 103, 7743.
10. A. B. Fuertes and D. M. Nevskaia, *J. Mater. Chem.*, 2003, 13, 1843.
11. L. A. Rodrigues, M. L. C. P. d. Silva, M. O. Alvarez-Mendes, A. d. R. Coutinho and G. P. Thim, *Chem Eng j*, 2011, 174, 49-57.
12. H. Tamai, T. Kakii, Y. Hirota, T. Kumamoto and H. Yasuda, *Chem. Mater.*, 1996, 8, 454.
13. R. J. Littel, G. F. Versteeg and W. P. M. Swaaij, *Chem. Engg. Sci.*, 1991, 46, 3308-3313.
14. S. Bishnoi and G. T. Rochelle, *Chem. Engg. Sci.*, 2000, 55, 5531-5543.
15. A. Aroonwilas and A. Veawab, *Ind. Eng. Chem. Res.*, 2004, 43, 2228-2237.
16. S. Choi, J. H. Drese and C. W. Jones, *ChemSusChem*, 2009, 2, 796-854.
17. A. Sayari, Y. Belmabkhout and R. Serna-Guerrero, *CHem. Engg. J.*, 2011, 171, 760-774.
18. G. M. Plaza, S. Garcia, F. Rubiera, J. J. Pis and C. Pevida, *CHem. Engg. J.*, 2010, 163, 41-47.
19. Q. A. Wang, J. Z. Luo, Z. Y. Zhong and A. Borgna, *Energy Environ. Sci.*, 2011, 4, 42-55.
20. X. Liu, J. L, L. Zhou, D. Huang and Y. Zhou, *Chem. Phys. Lett.*, 2005, 415, 198-201.
21. Y. Sun, X. W. Liu, W. Su, Y. Zhou and L. Zhou, *Appl. Surf. Sci.*, 2007, 253, 5650-5655.
22. T. L. Chew, A. L. Ahmed and S. Bhatia, *Adv. Colloid Interface Sci.*, 2010, 153, 43-57.
23. A. R. Millward and O. M. Yaghi, *J. Am. Chem. Soc.*, 2005, 127, 17998-17999.
24. Q. Yang, C. Zhong and J. F. Chen., *J. Phys. Chem. C*, 2008, 112, 1562-1569.
25. R. Banerjee, H. Furukawa, D. Britt, C. Kobler, M. O'Keeffe and O. M. Yaghi, *J. Am. Chem. Soc.*, 2009, 131, 3875-3877.
26. S. R. Caskey, A. G. Wong-Foy and A. J. Matzger, *J. Am. Chem. Soc.*, 2008, 130 10870-10871.
27. L. Bastin, P. S. Barcia, E. J. Hurtado, J. A. C. Silva, A. E. Rodrigues and B. Chen, *J. Phys. Chem. C*, 2008, 112, 1575-1581.
28. B. Liu and B. Smit, *Langmuir*, 2008, 25 5918-5926.
29. H. Furukawa and O. M. Yaghi, *J. AM. CHEM. SOC.*, 2009, 131, 8875–8883.
30. M. Cinke, J. Li, C. W. Bauschlicher, A. Ricca and M. Meyyappan, *Chem. Phys. Lett.*, 2003, 376, 761-766.
31. D. N. Futaba, K. Hata, T. Namai, T. Yamada, K. Mizuno, Y. Hayamizu, M. Yumura and S. Iijima, *J. Phys. Chem. B*, 2006, 110, 8035−8038.
32. D. N. Futaba, K. Hata, T. Yamada, T. Hiraoka, Y. Hayamizu, Y. Kakudate, O. Tanaike, H. Hatori, M. Yumura and S. Iijima, *Nat. Mater.*, 2006, 5, 987-994.
33. T. Yamada, T. Namai, K. Hata, D. N. Futaba, K. Mizuno, J. Fan, M. Yudasaka, M. Yumura and S. Iijima, *Nat. Nanotechnol.*, 2006, 1, 131-136.
34. M. Rahimi, J. K. Singh, D. J. Babu, J. J. Schneider and F. Muller-Plathe, *J Phys Chem C*, 2013, 117, 13492-13501.
35. W.-Q. Deng, X. Xu and W. Goddard, *Phys. Rev. Lett.*, 2004, 92, 166103.
36. M. Rahimi, J. K. Singh and F. M. Plathe, *J. Phys. Chem. C*, 2015, 119, 15232–15239.
37. S. H. Joo, S. J. Choi, I. Oh, J. Kwak, Z. Liu and O. Terasaki, *Nature*, 2001, 412, 169-172.
38. M. Kruk, M. Jaroniec, T. W. Kim and R. R. R, *Chem Mater*, 2003, 15, 2815-2823.
39. T. Kim, M. Kim, Y. Yang, J. Kim, S. Jeong and C. Kim, 2015, 40, 15236-15243.
40. R. J. M. Pellenq, S. Rodts, V. Pasquier, A. Delville and P. Levitz, *Adsorption*, 2000, 6, 241.
41. B. Coasne, F. R. Hung, R. J. M. Pellenq, F. R. Seperstein and K. E. Gubbins, *Langmuir*, 2006, 22, 194.
42. R. J.-M. Pellenq and D. Nicholson, *J. Phys. Chem.*, 1994, 98, 13339.
43. D. W. Brenner, *Phys. Rev. B*, 1990, 42, 9458.
44. X. Peng, D. P. Cao and W. C. Wang, *Langmuir*, 2009, 25, 10863.
45. J. J. Potoff and J. I. Siepmann, *AIChE J.*, 2001, 47, 1676–1682.
46. M. Kim and J. Chang, 2015, 32, 939-949.
47. W. L. Jorgensen, J. M. Briggs and M. L. Conteras, *J. Phys. Chem.*, 1990, 94, 1683.
48. J. G. Harris and K. H. Yung, *J. Phys. Chem.*, 1995, 99, 12021-12024.
49. H. A. Lorentz, *Annalen der Physik*, 1881, 12, 127-136.
50. S. J. Mahdizadeh and S. F. Tayyari, *Theor. Chem. Acc.*, 2011, 128, 231-240.
51. D. D. Do and H. D. Do, *J. Phys. Chem. B*, 2006, 110.
52. Z. Liua, T. Horikawa, D. D. Do and D. Nicholson, *J. Colloid Interface Sci.*, 2012, 368, 474-487.
53. A. L. Myers and P. A. Monson, *Langmuir*, 2002, 18, 10261-10273.
54. T. Vuong and P. A. Monson, *Langmuir*, 1996, 12, 5425-5432.
55. W. Humphrey, A. Dalke and K. Schulten, 1996, 14, 33-38.
56. S. K. Jain, R. J.-M. Pellenq, J. Pikunic and K. E. Gubbins, *Langmuir*, 2006, 22, 9942.
57. S. K. Jain and K. E. Gubbins, *Langmuir*, 2007, 23, 1123.
58. G. R. Birkett and D. D. Do, *J. Phys. Chem. C*, 2007, 111, 5735.
59. L. Zhou, X. Liu, J. Li, N. Wang, Z. Wang and Y. Zhou, *Chem. Phys. Lett.*, 2005, 413, 6-9.
60. X. Peng, D. Cao and W. Wang, *Chem. Engg. Sci.*, 2011, 66, 2266-2276.
61. L. Huang, L. Zhang, Q. Shao, L. Lu, X. Lu, S. Jiang and W. Shen, *J. Phys. Chem. C*, 2007, 111, 11912–11920.
62. P. Kowalczyk, S. Furmaniak, P. A. Gauden and A. P. Terzyk, *J. Phys. Chem. C*, 2010, 114, 21465-21473.
63. M. Rzepka and P. Lamp, *J. Phys. Chem. B*, 1998, 102, 10894–10898.
64. X. Peng, D. Cao and W. Wang, *J. Phys. Chem. C*, 2008, 112, 13024–13036.